

CuTe Nanocrystals: Shape and Size Control, Plasmonic Properties, and Use as SERS Probes and Photothermal Agents

Supporting Information

Wenhua Li,[†] Reza Zamani,^{†,£} Pilar Rivera_Gil,^Ψ Beatriz Pelaz,^Ψ Maria Ibáñez,[‡] Doris Cadavid,[†] Alexey Shavel,[†] Ramon A. Alvarez-Puebla,^{§,Σ,§} Wolfgang J. Parak,^Ψ Jordi Arbiol,^{£,§} and Andreu Cabot^{*,†,‡}

[†] Catalonia Energy Research Institute - IREC, Jardí de les Dones de Negre 1, Sant Adria del Besos, Barcelona, 08930, Spain,

[£] Institut de Ciència de Materials de Barcelona, ICMA-B-CSIC, Campus de la UAB, Bellaterra, 08193, Spain.

^Ψ Philipps Universität Marburg, Marburg, Germany

[§] Department of electronic Engineering, Universitat Rovira i Virgili, Tarragona, Spain

^Σ Center for Chemical Technology of Catalonia, Tarragona Spain

[‡] Departament d'Electrònica, Universitat de Barcelona, Barcelona, 08028, Spain.

[§] Institució Catalana de Recerca i Estudis Avançats (ICREA), 08010 Barcelona, Spain.

Table of Contents

1. Materials and Methods.....	S2
1.1. Materials.....	S2
1.1.1. Chemicals and solvents.....	S2
1.2. Methods.....	S2
1.2.1. CuTe nanocubes.....	S2
1.2.2. CuTe nanocubes size control.....	S2
1.2.3. CuTe nanoplates:.....	S2
1.2.4. CuTe nanorods:.....	S2
1.2.5. Synthesis of tris[bis(trimethylsilyl)amido] copper(I).....	S3
1.3. Characterization techniques.....	S3
2. Additional Nanoparticles Characterization.....	S4
2.1. Shape and size evolution with reaction time.....	S4
2.2. Control experiments: LiN(SiMe ₃) ₂ role.....	S4
2.3. Nanocubes size control.....	S5
2.4. Nanoplates shape.....	S6
2.5. Nanorods at longer reaction times.....	S7
2.6. Composition.....	S8
2.7. Crystal structure.....	S9
2.8. UV-vis spectroscopy.....	S10
3. Surface Enhanced Raman Spectroscopy:.....	S11
4. Polymer coating CuTe nanoparticles:.....	S13
5. Cell culture and laser irradiation.....	S15

1. Materials and Methods

1.1. Materials

1.1.1. Chemicals and solvents

Copper (I) chloride (reagent grade, 97 %), Lithium bis(trimethylsilyl) amide ($\text{LiN}(\text{SiMe}_3)_2$, 97 %), oleylamine (OLA), octadecene (ODE, 90 %), oleic acid (OA, tech. 90 %), tellurium shots (99.999 %), were all purchased from Aldrich. Trioctylphosphine oxide (TOPO, 99 %), tri-n-octylphosphine (TOP, 97 %) were purchased from Strem. Chloroform, isopropanol and tetrachloroethylene (TCE, $\geq 99\%$, Aldrich) were of analytical grade and obtained from various sources. All chemicals were used as received without further purification except OLA. All syntheses were carried out using standard airless techniques: a vacuum/dry argon gas Schlenk line was used for the syntheses and an argon glove-box for storing and handling air and moisture-sensitive chemicals.

1.2. Methods

1.2.1. CuTe nanocubes

In a typical synthesis, 0.25 mmol (0.025 g) of CuCl was mixed with 1 mmol of TOPO (0.3866 g) and 6 mL of OLA in a 25 mL three-neck flask. The reaction mixture was kept under vacuum (~ 0.1 mbar) in the Schlenk line for 20 min at room temperature and then heated to 100 °C to obtain a clear blue solution. To remove low boiling point impurities, the solution was maintained at 100 °C under vacuum for 30 min and it was periodically flushed with argon. Then temperature was increased to 160 °C under argon and a light clear yellow solution was obtained. At this temperature, 0.125 mL of TOP was added and temperature was allowed to recover to 160 °C. In parallel, a tellurium precursor solution was prepared inside the glovebox by mixing 0.125 mL of a 2 M TOPTe (0.25 mmol) solution with 0.5 mL of a 0.5 M $\text{LiN}(\text{SiMe}_3)_2$ solution in dried ODE. The tellurium precursor solution was rapidly injected to the copper solution maintained at 160 °C, which immediately changed color, from light yellow to deep green. Upon injection, the temperature of the reaction mixture dropped to 152 °C. At this point, temperature was set to 220 °C and nanoparticles were allowed to grow for 30 min. Afterward, the colloidal solution was rapidly cooled to room temperature with a water bath at the rate of ~ 80 °C/min. While cooling, when temperature reached approximately 70 °C, 2 mL of oleic acid were added to replace the weakly bound OLA molecules. The crude solution was mixed with 5 mL of chloroform and sonicated for 5 min. The CuTe nanoparticles were isolated by centrifugation at 6000 rpm during 6 min. The deep green precipitate was redispersed in chloroform (~ 5 mL) and sonicated for 1 min. Then the product was precipitated once more by centrifugation in the presence of isopropanol (~ 10 mL). The nanoparticles were re-dispersed in chloroform (~ 5 mL) and stored in glovebox until their posterior use.

1.2.2. CuTe nanocubes size control

The same procedures were carried out to get the nanocubes with different size, except that different amount of CuCl was used instead of 0.25 mmol (Cu:Te as 1:1) as described above. The lower the nominal Cu:Te ratio, the smaller the nanocube size. The Cu amounts used were: 0.1875 mmol (Cu:Te = 3:4), 0.125 mmol (Cu:Te = 1:2). Herein, it is worth to mention that the optimal amount of Te precursor is 0.25 mmol to obtain the monodisperse nanocubes.

1.2.3. CuTe nanoplates:

Optimized copper telluride nanoplates were prepared following the same procedure but reducing the reaction temperature to 190 °C and the growth time to 15 min.

1.2.4. CuTe nanorods:

Optimized copper telluride nanorods were obtained following the procedure but adding 0.75 mL TOP instead of 0.25 mL and setting the growth temperature to 190 °C and the growth time to 2 min.

1.2.5. Synthesis of tris[bis(trimethylsilyl)amido] copper(I)

$\text{CuN}(\text{SiMe}_3)_2$ is a light-yellow powder, soluble in hydrocarbons and ethers. Its synthesis by a metathesis reaction between CuCl and $\text{LiN}(\text{SiMe}_3)_2$ was inspired by the originally proposed preparation of $\text{Bi}[\text{N}(\text{SiMe}_3)_2]_3$ by C. J. Carmalt et al.¹ All steps of synthesis were carried under air-less conditions using anhydrous solvents. 10 mmol (1.673 g) of $\text{LiN}(\text{SiMe}_3)_2$ was dissolved in 20 mL of diethyl ether, and cooled to 0 °C. An exactly equimolar amount of CuCl (3 mmol, 0.297 g) dissolved in a mixture of diethylether (20 mL) and tetrahydrofuran (10 mL) were then slowly added, resulting in a yellow turbid solution. The mixture was stirred additionally for 2 hours, centrifuged to remove LiCl and filtered through a PTFE filter (pore size 450 nm). All solvents were removed by vacuum for at least 1 hour. The resulting yellow powder was re-dissolved in pentane (15 mL). The solution was filtered and evaporated using vacuum again. The obtained $\text{CuN}(\text{SiMe}_3)_2$ was stored inside the glovebox.

1.3. Characterization techniques

Transmission Electron Microscopy (TEM) and high-resolution TEM (HRTEM): The morphological, chemical and structural characterizations of the nanoparticles were carried out by TEM, HRTEM, electron energy loss spectroscopy (EELS). Carbon-coated TEM grids from Ted-Pella were used as substrates. HRTEM images were obtained using a Jeol 2010F field-emission gun microscope with a 0.19 nm point-to-point resolution at 200 keV with an embedded Gatan image filter for EELS analyses. Images were analyzed by means of Gatan Digital micrograph software. Particle size distributions were obtained by measuring at least 150 NPs per each sample.

Scanning Electron Microscopy (SEM): The measurement was performed using a ZEISS Auriga SEM with an energy dispersive X-ray spectroscopy (EDX) detector at 20 kV to study the composition of nanoparticles. The particles were cleaned very well and dissolved in chloroform. The samples were prepared by dropping the solution on the clean Silicon substrates.

Powder X-ray Diffraction patterns (XRD): The powder XRD patterns were obtained with $\text{Cu K}\alpha$ ($\lambda = 1.5406 \text{ \AA}$) radiation in reflection geometry on a Bruker D8 operating at 40 kV and 40 mA.

Ultraviolet-Visible Spectrophotometry (UV-Vis): Optical absorption spectra were recorded on a LAMBDA 950 UV-Vis spectrophotometer from PerkinElmer.

2. Additional Nanoparticles Characterization

2.1. Shape and size evolution with reaction time

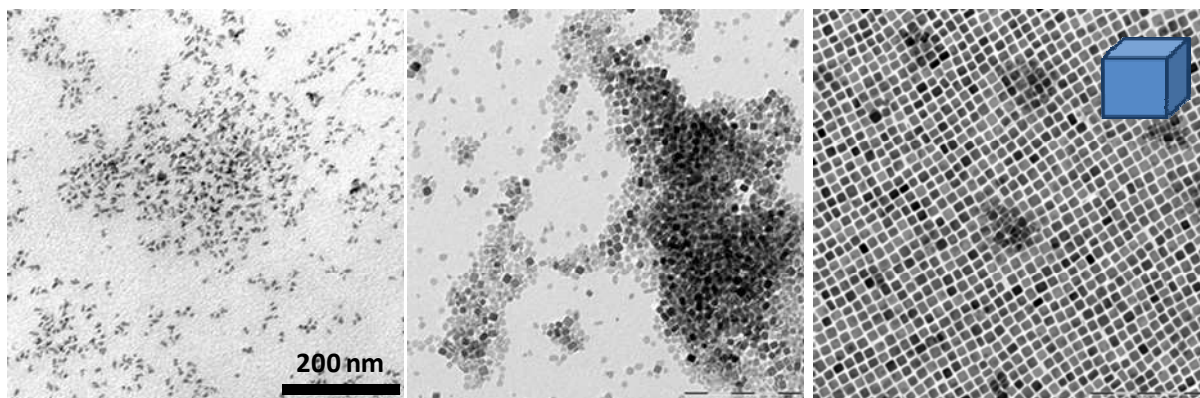


Figure S1. TEM micrographs showing the size and shape evolution of copper telluride nanocubes at reaction times of 3 min, 15 min and 30 min.

2.2. Control experiments: $\text{LiN}(\text{SiMe}_3)_2$ role

To assess the role of $\text{LiN}(\text{SiMe}_3)_2$ we prepared CuTe nanoparticles following the exact same procedure but without $\text{LiN}(\text{SiMe}_3)_2$. Figure S2 left shows the large particles obtained.

To further assess the lithium role in the size and shape control, we prepared $\text{CuN}(\text{SiMe}_3)_2$ and used this precursor for the Li-free synthesis of CuTe nanoparticles. Without $\text{LiN}(\text{SiMe}_3)_2$, quasi-spherical nanoparticles were obtained (Figure S2 right), proving the important role of $\text{LiN}(\text{SiMe}_3)_2$ on determining the nanocrystals shape.

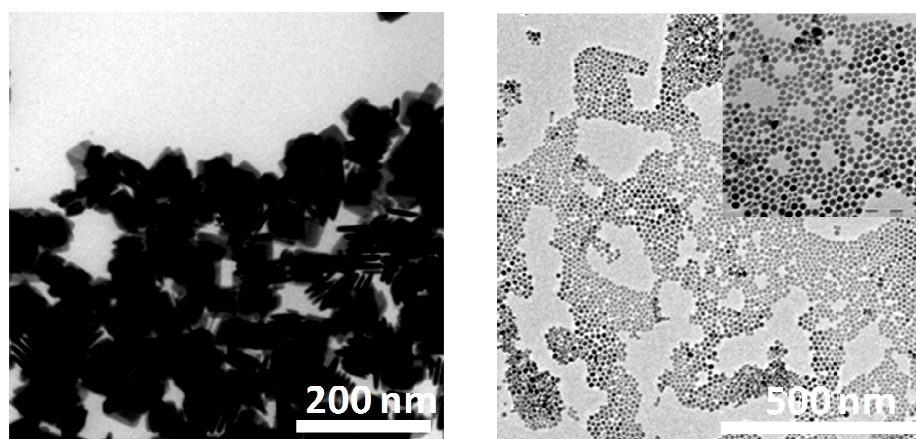


Figure S2. TEM micrographs showing the nanoparticles obtained without $\text{LiN}(\text{SiMe}_3)_2$ (left) and using $\text{CuN}(\text{SiMe}_3)_2$ as Cu precursor in the absence of Lithium (right).

2.3. Nanocubes size control

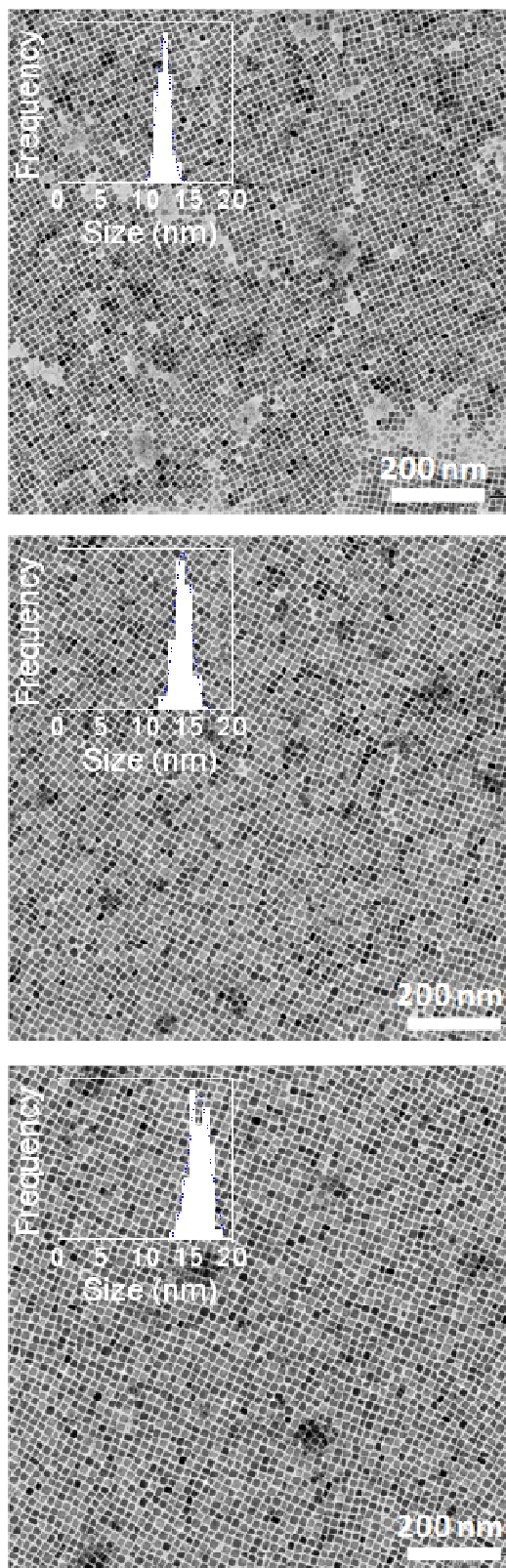


Figure S3. TEM micrographs of CuTe nanocubes with different average size obtained from different Cu:Te ratios (from top to bottom, the nominal Cu:Te ratio are 1:2, 3:4 and 1:1, respectively).

2.4. Nanoplates shape

The left HRTEM image in Figure S4 shows three nanoplates aligned by their length. The one in the middle is lying on its side, meaning that the dimensions we see are the thickness (6 nm) and the length (18 nm), while the other two are lying on the largest surface, meaning we can see their widths (10 nm) and lengths (16 and 17 nm). The right HRTEM image in Figure S4 also shows few CuTe nanoplates. The nanoplate in the middle is lying on its widest side (12x21 nm), and the top-right nanoplate in the same image is lying on its side and has a thickness of around 7 nm. Notice the surface gets slightly rough under the TEM e-beam.

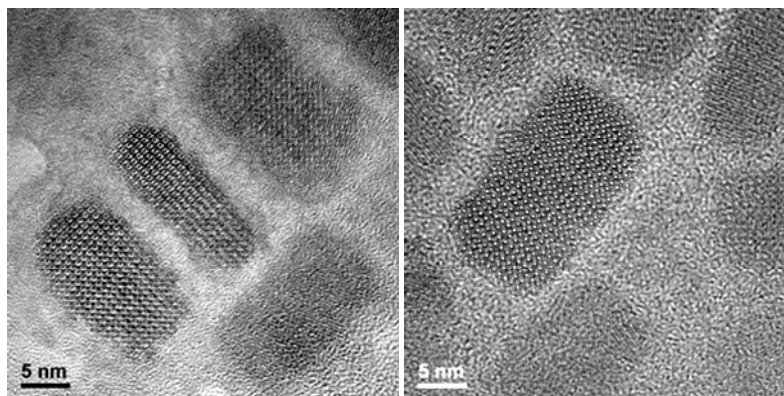


Figure S4. HRTEM micrographs of CuTe nanoplates.

In the HAADF images the brightness is proportional to the material composition and also to the sample thickness (linear density). As all nanoplates have the same chemical composition, the intensity profiles of the HAADF images are related to their thickness of the plates we see. In the images below we show the HAADF 3D (Figure S5) and 1D (Figure S6) intensity profiles of the CuTe NPs oriented in different directions, some of them are lying on the thin side, and others are lying on the widest side. The bimodal distribution of thicknesses obtained probes that the geometry of the CuTe nanostructures obtained is the plate.

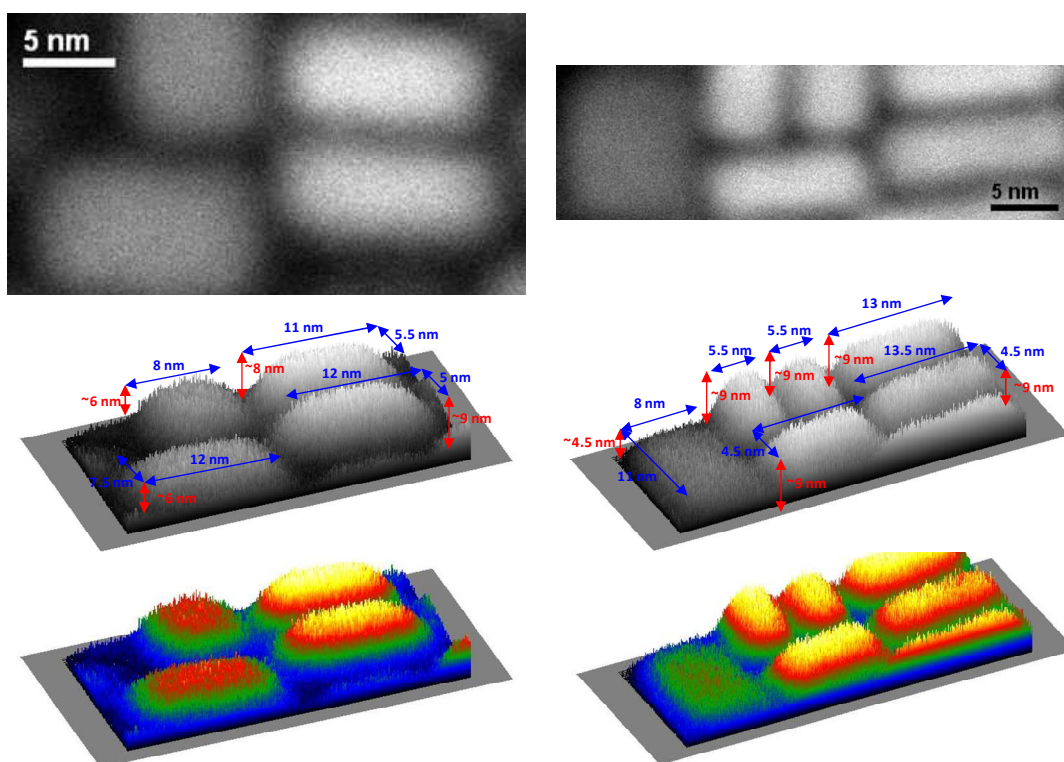


Figure S5. HAADF images and 3D profiles of CuTe nanoplates.

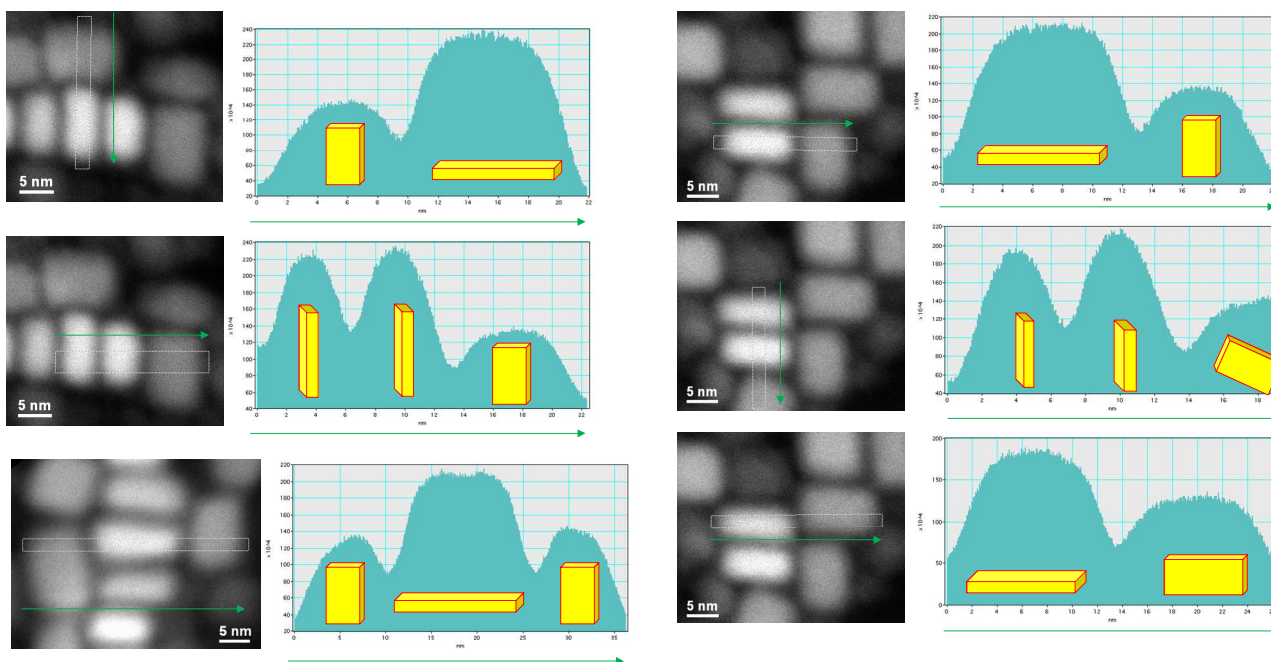


Figure S6. HAADF images and intensity profiles of CuTe nanoplates.

2.5. Nanorods at longer reaction times

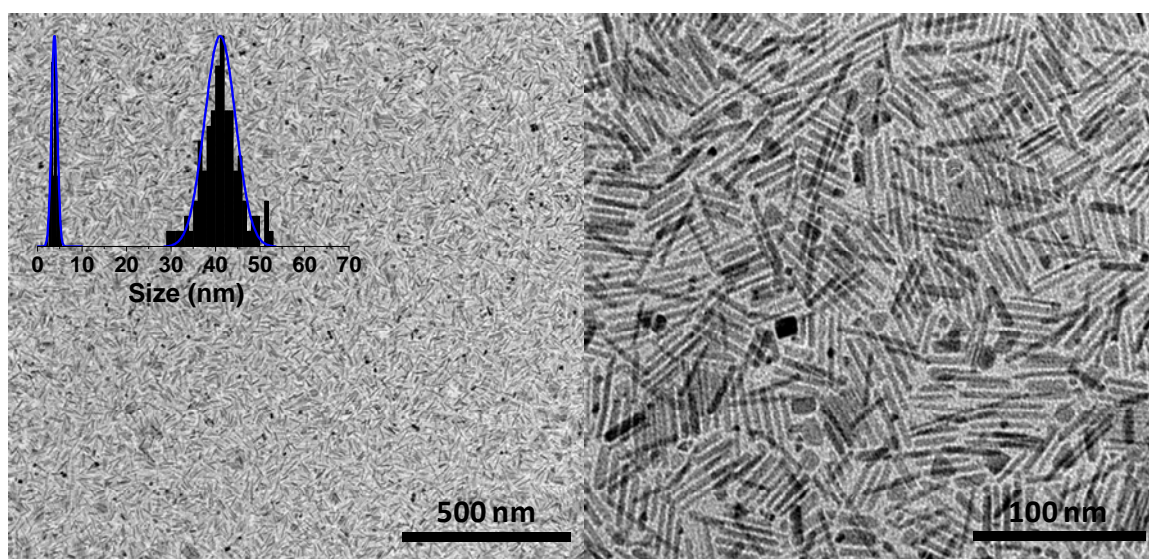


Figure S7. TEM micrographs of CuTe nanorods obtained as detailed in the manuscript after 5 min reaction time.

2.6. Composition

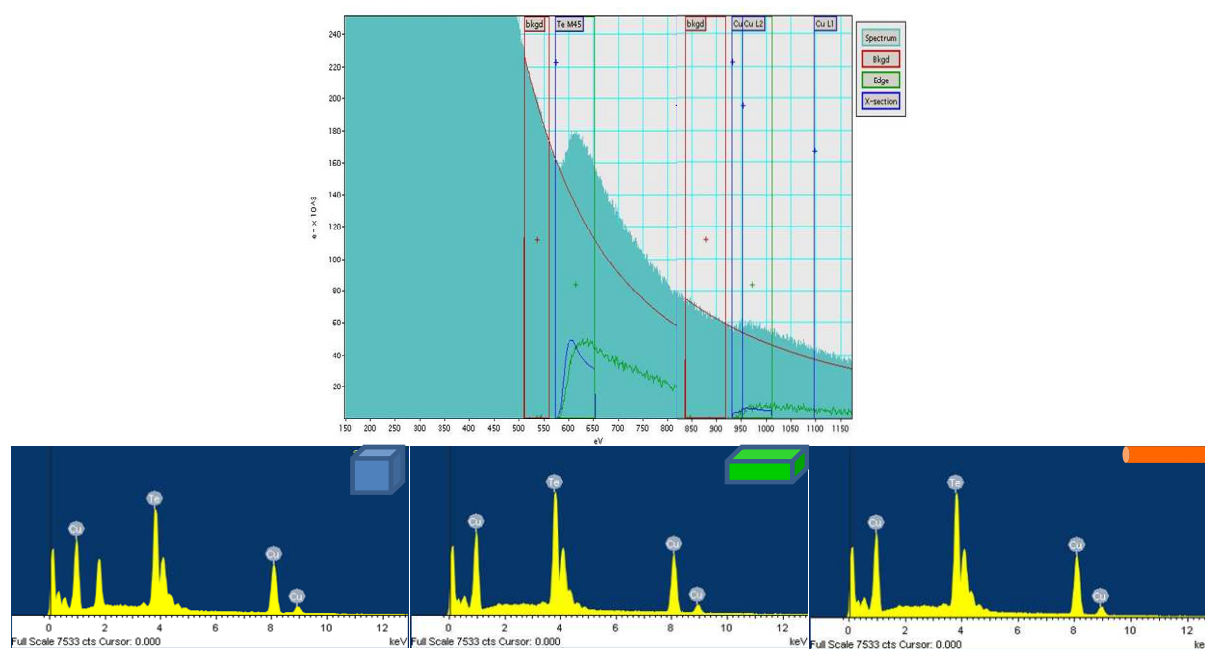


Figure S8. Raw EELS spectrum (top) and EDX spectra (bottom) of copper telluride nanoparticles and the quantification on parent-spectrum image shows the nanoparticle composition to be 52% of Cu and 48% of Te, with a 4% error, taking into account the technique resolution and statistical variations from sample to sample. Thus the ratio Cu:Te is very close to 1:1, which is consistent with the results obtained from an extensive EDX analysis of numerous samples. In the EELS analysis, the width of the signal windows was 80 eV in the case of both elements (in the case of Te starting from 572 eV, and in the case of Cu starting from 931 eV).

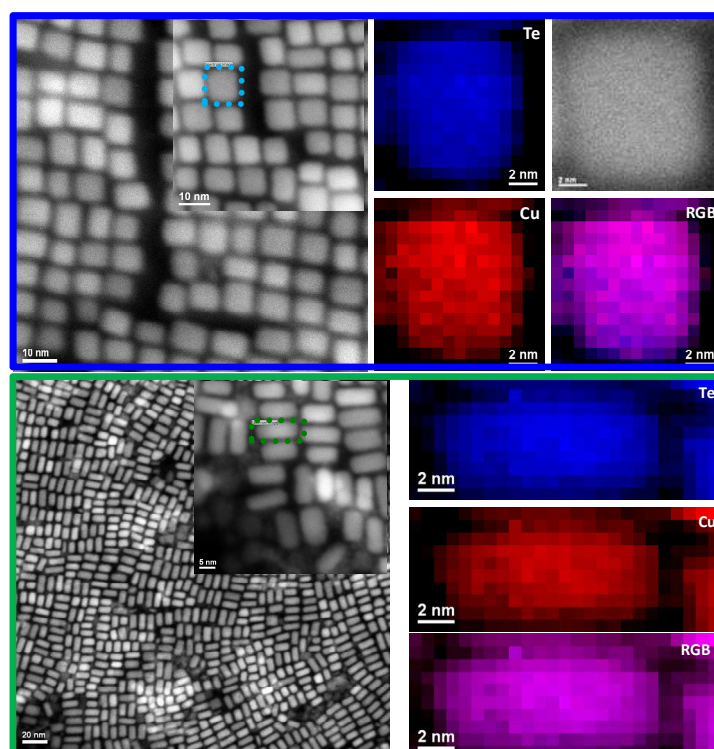


Figure S9. Z-contrast scanning TEM images and Te and Cu EELS elemental mapping images of copper telluride nanocubes and nanoplates.

2.7. Crystal structure

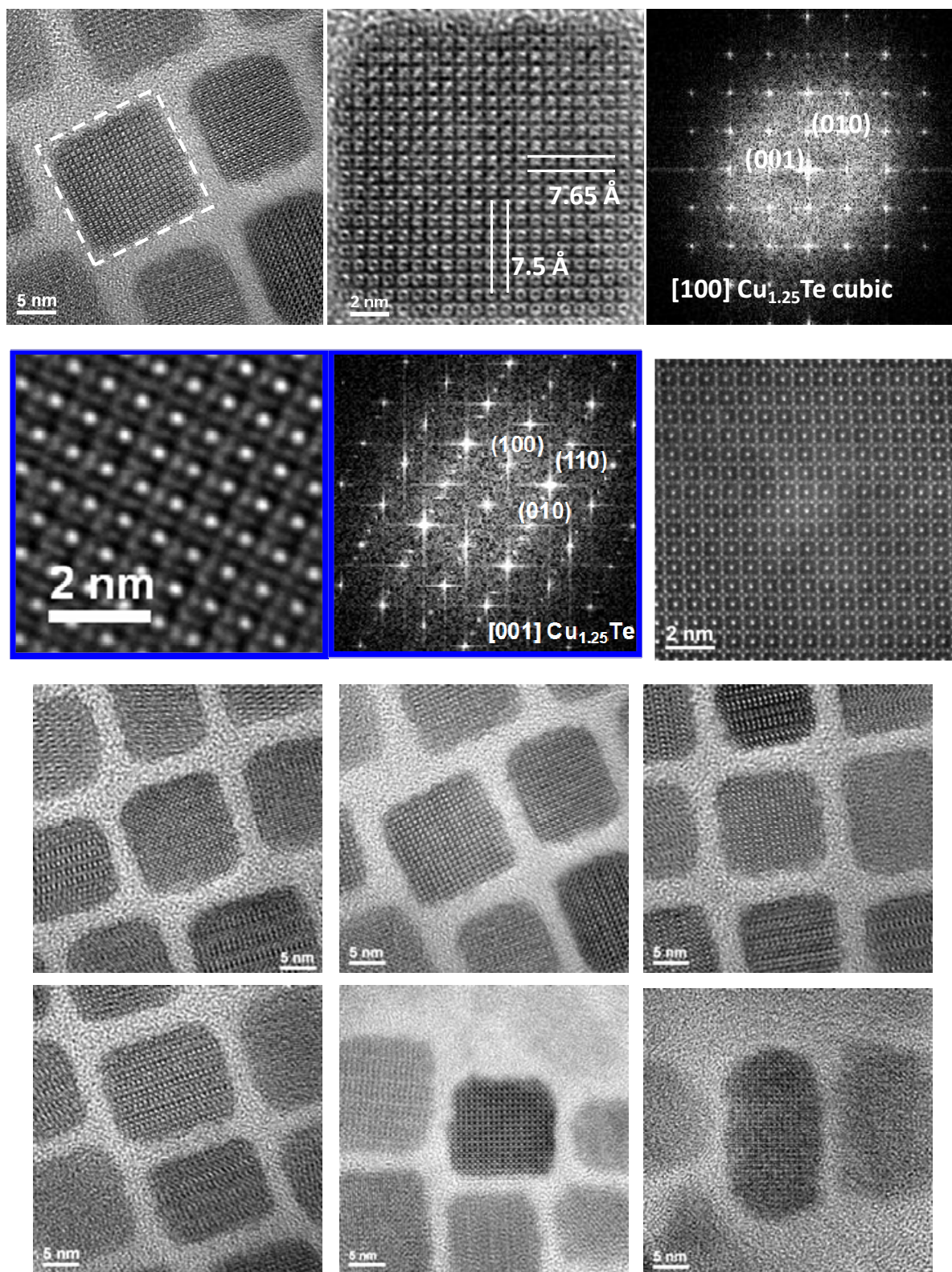


Figure S10. HRTEMs and power spectra of copper telluride nanocrystals (top 2 lines), annular dark-field scanning TEM image (second line) and additional HRTEM micrographs of CuTe nanoparticles. The crystal structure resembles that of a tetragonal $\text{Cu}_{1.25}\text{Te}$ phase with cell parameter $a=b=7.50\pm 0.05\text{\AA}$ and $c=7.65\pm 0.05\text{\AA}$ nm. However, periodic spots appearing between the main spots indicate the presence of an ordered superstructure.

2.8. UV-vis spectroscopy

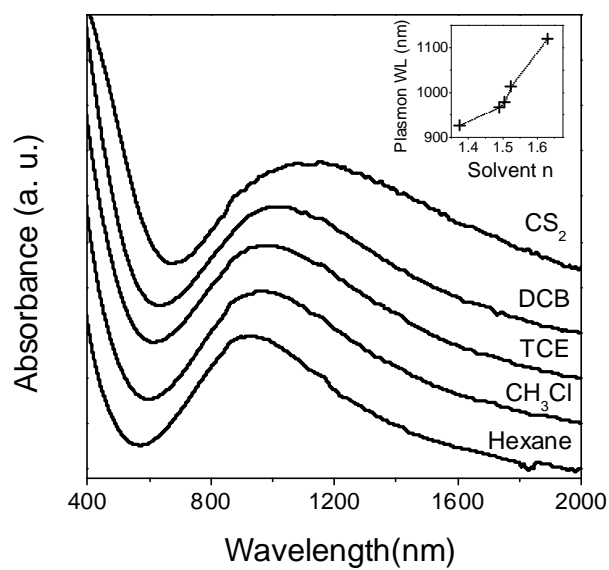


Figure S11. UV-vis spectra of copper telluride nanocubes in different solvents. Inset displays the peak position as a function of the solvent.

3. Surface Enhanced Raman Spectroscopy:

SERS experiments were carried out on 250 μL solutions containing 0.17 g L^{-1} of particles (either CuTe or Au) alone (Figure S12) and with minute concentrations of analytes. Briefly, 2.5 μL of analyte in acetone (10^{-5} M) were added to 1 mL of particles in chloroform giving rise to a final concentration of 10^{-7} M. The samples were studied in solution by using a macrosampler adaptor with 15 mm working distance macro-objective. The inelastic scattering was collected with a Renishaw Invia system by exciting the samples with 830 nm laser line for 10 s and a power at the sample of 89 mW. Gold nanostars were produced by following standard methods (Ref 9 in manuscript, Figure S13)

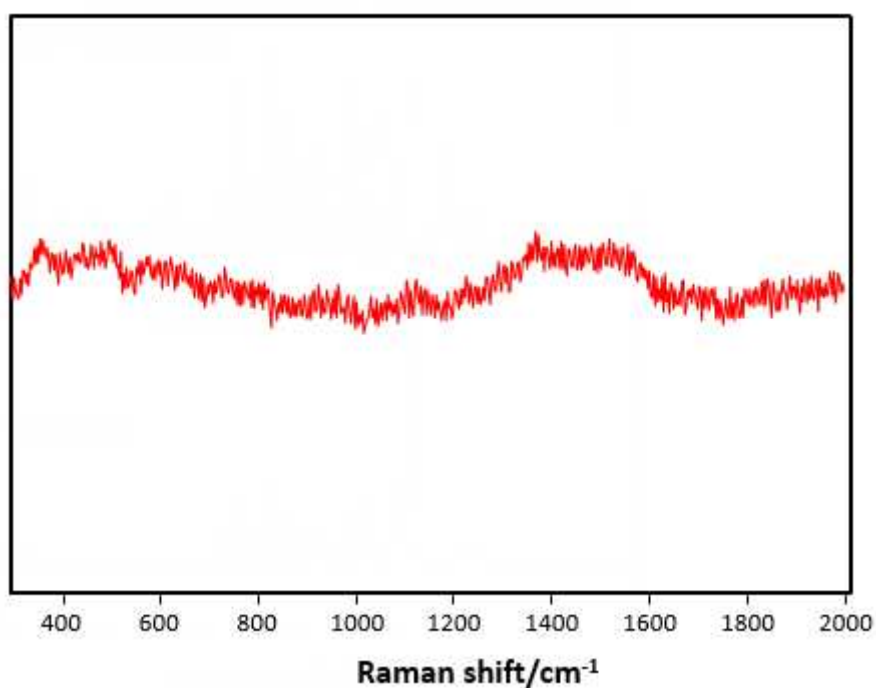


Figure S12. SERS spectra of the colloidal suspensions of CuTe without any analyte.

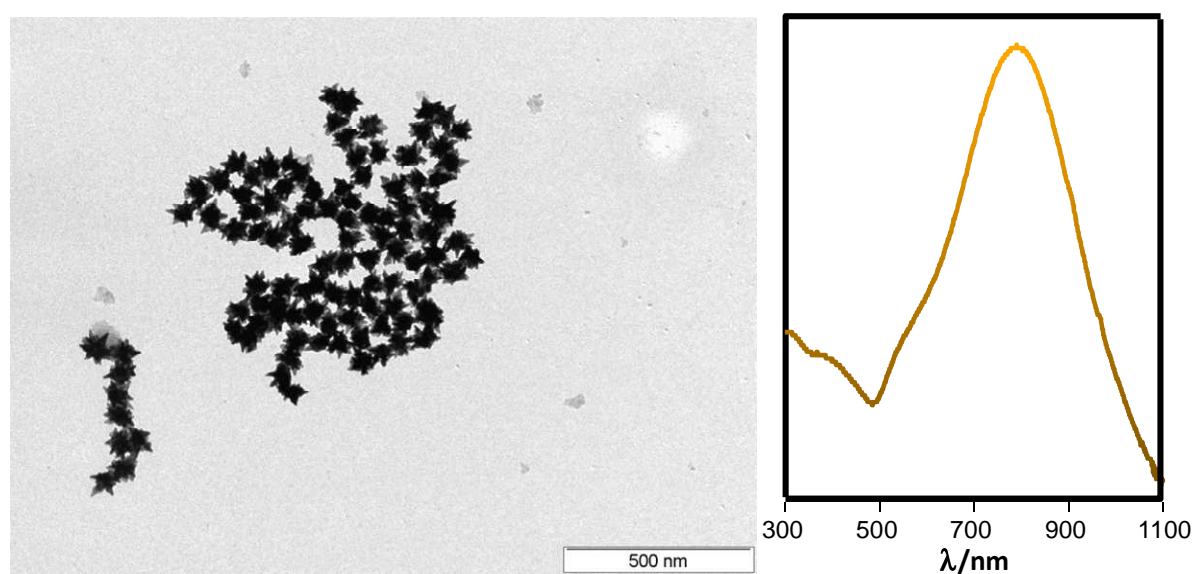


Figure S13. TEM image of gold nanostars and their UV-vis spectrum showing the plasmonic absorption.

For a given excitation wavelength, the SERS intensity is related to the absolute square electromagnetic field outside the particle and is enhanced, with respect to the Raman intensity, by a factor (EF):

$$EF_{(\lambda)} = \frac{|E_{out(\lambda)}|^2 |E_{out(\lambda-\lambda_s)}|^2}{E_0^4} = \frac{I_{SERS}}{I_R} f \quad (2)$$

Where $E_{out(\lambda)}$ and $E_{out(\lambda-\lambda_s)}$ are the electromagnetic fields generated by the incident excitation and the Stokes' shifted Raman. The use of the first term of the equation for the calculation of the enhancement factor results difficult, thus, experimentally, EF is usually calculated by direct comparison of the intensities provided by the SERS and Raman experiments and normalized by the total number of molecules (N) in each experiment ($f = N_R/N_{SERS}$).² In our case, a concentrated solution of Nile red (10^{-2} M in acetone) was measured under the same conditions that the experiments carried out nanoparticles.

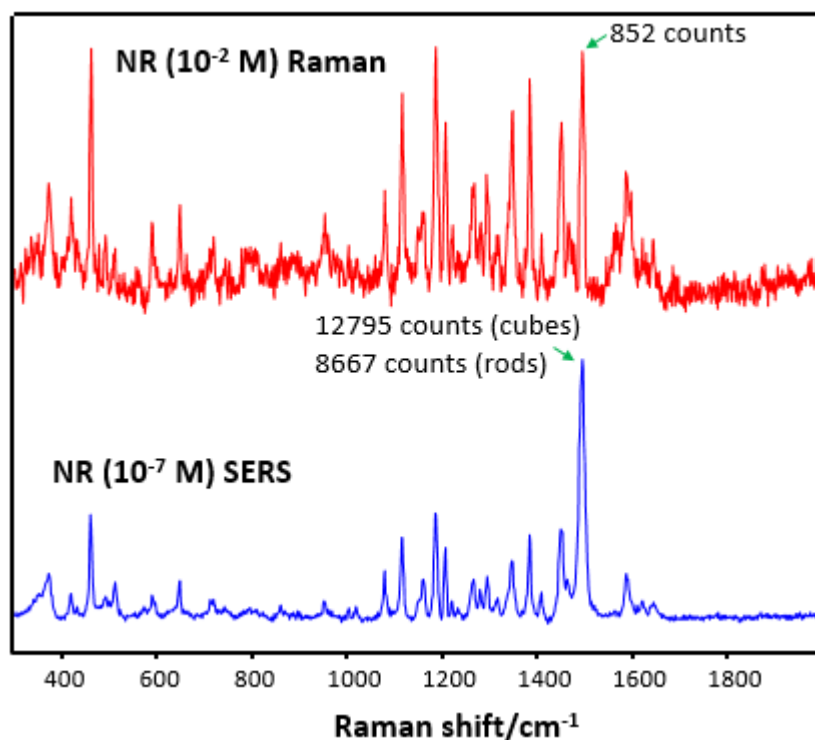


Figure S14. Raman and SERS spectra of a Nile red.

4. Polymer coating CuTe nanoparticles:

The cubic CuTe nanoparticles (NPs) with length of 16 nm were transferred to the aqueous phase using the polymer coating methodology, as previously described by Pellegrino et al.³ This methodology was adapted based on the overall surface area of the CuTe NPs, aiming effectively to coat all the NPs. That is, it has to be adjusted taking into consideration the surface area per single cubic CuTe NP (A_0) and then, the total surface area (A) to coat. To calculate the surface area for single NP, an effective length was used (d_{eff}). This length is the result of the addition of the length observed in the TEM measurements ($d_{core}= 16$ nm) and two times the assumed thickness of the surfactant shell ($d_{surfactant}= 1$ nm). The amount of polymer needed to stabilize the NPs was optimized, yielding best results using 1000 polymer monomers per nm^2 ($r_{P/Np}$). (Formulas (1) and (2))

$$A_0 = 6 \times (d_{core} + 2d_{surfactant}) \times (d_{core} + 2d_{surfactant}) = 6 \times d_{eff}^2 \quad (1)$$

$$A = C \times V \times N_A \times A_0 \quad (2)$$

Where: A_0 is the surface area of single cubic nanoparticle (nm^2); A is the total surface area of all the colloidal nanoparticles in the solution (nm^2); d_{core} is the length of the side of the particles; $d_{surfactant}$ correspond with thickness of the surfactant layer on NPs surface; d_{eff} is the total length; V refers to the volume of solution of NPs (L) and N_A is the Avogadro constant.

The amphiphilic polymer used is formed by a backbone of poly(isobutylene-*alt*-maleic anhydride) (PMA, Mw=6000 g/mol, SigmaAldrich; each polymer chain contains approximately 39 monomer units) derivatized with dodecylamine in order to have an aliphatic domain. The polymer presents a 75% of the anhydrides modified with dodecylamine. The procedure was described by Lin et al.⁴ The amount of polymer which is needed to coat the particles was estimated by formula (3).

$$V_P = \frac{N_P}{C_P} = \frac{A \times r_{P/Np}}{N_A C_P} \quad (3)$$

Where, V_p is the volume of polymer needed to coat the NPs; N_p , number of NPs mol (mol); C_p , concentration of polymer (M); A is the total surface area of nanoparticles to coat (nm^2) and $r_{P/Np}$ is the ratio of monomer per nm^2 needed to stabilize efficiently the particles and N_A is the Avogadro constant.

In the case of the coating 500 μ L (V) of the CuTe NPs with 16 nm in length ($d_{eff}= (16+2)= 18$ nm) with a concentration of 0.1 μ M (C), taking a ratio of the monomer as 1000 monomer per nm^2 , the surface per NP (A_0) will be equal to 1944 nm^2 and the total surface area (A) in the 500 μ L of CuTe NPs solution will be $5.85 \times 10^{16} nm^2$. It was determined experimentally that 1000 monomer/ nm^2 ($r_{P/Np}$) represents a good value to provide the NPs with colloidal stability. Finally, using the Formula 3, the volume required for polymer (V_p) of 0.05 M (C_p) is 1.95 mL.

The NPs and the polymer were placed together in a round flask, and diluted with chloroform. After 10-20 min, the chloroform was slowly evaporated under reduced pressure by a rotavapor system (Laborota 4000, Heidolph) using 70 °C in the bath.⁵ The resulting solids were quickly dissolved in basic buffer solution (0.1 M NaOH) to drive the nanoparticles to the aqueous phase. To remove any big aggregate, the solution was filtrated through a syringe membrane filter (Roth # P818.1, 0.22 μ m pore size). Then the buffer was changed to water by the use of 100 kDa MWCO Amicon centrifuge filters (Millipore, Amicon Ultra-15, #UFC9100). The empty micelles generated by the excess of polymer were removed by gel electrophoresis (Sub-Cell GT electrophoresis cells, Bio-Rad). The previously concentrated nanoparticles were loaded into wells of a 2% agarose gel (Invitrogen #15510027) in 0.5 x TBE solution and gel electrophoresis was performed for one hour applying 100 V. The band which contained the nanoparticles was cut. The particles were extracted running again the electrophoresis, but this time, the gel-band was previously placed in a dialysis membrane (3500 Da MWCO, Roth). Finally, the NPs solution was filtered again by a syringe filter (0.22 μ m pores) to remove small gel pieces, and concentrated by 100 kDa MWCO Amicon centrifuge filters.

Figure S15a shows the absorption spectra of the NPs before (black line) and after (red line) the polymer coating of the NPs. Figure S15b corresponds with the gel electrophoresis in agarose 2% (100V, 1h) of the coated NPs and they were compared with a control sample, *i.e.* 10 nm gold NPs (see in the bottom). Finally Figure S15c presents a photograph of the final solution of the polymer coated CuTe NPs.

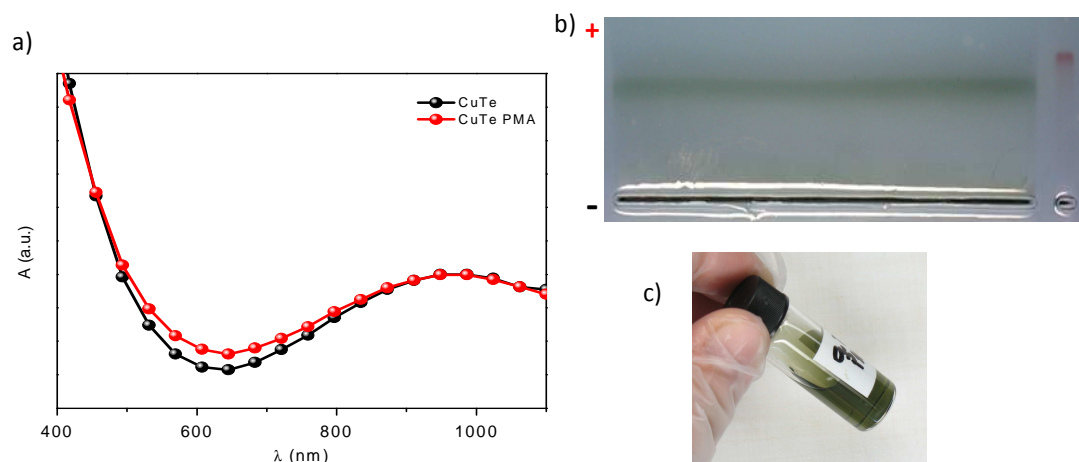


Figure S15. a) Absorption spectra of CuTe NPs before (black line) and after (red line) the polymer coating procedure. b) Gel electrophoresis image of the cleaning procedure of the CuTe NPs after their coating. Its electrophoretical mobility is compared with 10 nm Au NPs. c) Photograph of the final CuTe NPs solution after the polymer coating process and the cleaning steps.

The hydrodynamic radius and the ζ -potential value of the particles were also evaluated using a Malvern ZetaSizer. Particles showed a final hydrodynamic radius in number results 22.5 nm and a ζ -potential value of -55.6 mV. In both cases the standard deviation was less than a 5 %. (Figure S16)

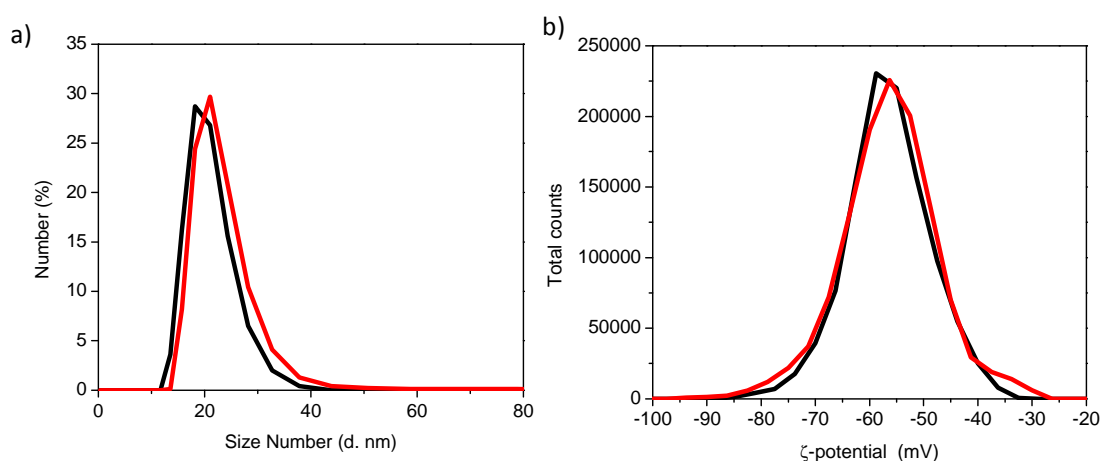


Figure S16. a) Radius hydrodynamic measurements in number; b) ζ -potential measurements, both from the final CuTe polymer coated NPs.

The concentration of the NPs was estimated as previously described by Rivera_Gil *et al.*,⁶ for any inorganic NP of known size, geometry and density. Taking into consideration size, shape and density, the molecular weight of the NPs can be determined in good approximation. In this particular case, particles are cubes of 16 nm of length composed by CuTe ($\rho_{\text{CuTe}} = 7.1 \text{ g/cm}^3$). The weight of one NP can be calculated using the density of the material and the volume of the particle. For a cubic NP the volume equation is the edge length (d_{core}) to the cubic power. In this case the volume for one particle in cm^3 is $5.088 \times 10^{-18} \text{ cm}^3$. This volume of one NP multiplied by the density of the material will give us the weight of one single NP. In this

case, one NP weight 3.61×10^{-17} g. The molecular weight for this NP will be the product of the weight of one NP by the Avogadro constant, e.g. 2.17×10^7 g/mol. Thus, a weighted mass of inorganic material (NPs in grams) can be used to give an approximated concentration (mol/L) of the NPs solution. For example, if 18.5 mg of CuTe NPs were dissolved in 8.5 mL of CHCl_3 , the final concentration of NPs will be approximately 0.1 μM .

Once the concentration is determined, using the absorption spectra, a standard curve can be done. In the actual sample, the standard curve was obtained using the absorbance of NPs solutions of known concentration of CuTe NPs at their maximum (950 nm). In the Figure S17 the standard curve to calculate the concentration is presented. So, using this approximation, it is possible to estimate the concentration of any solution of these NPs.

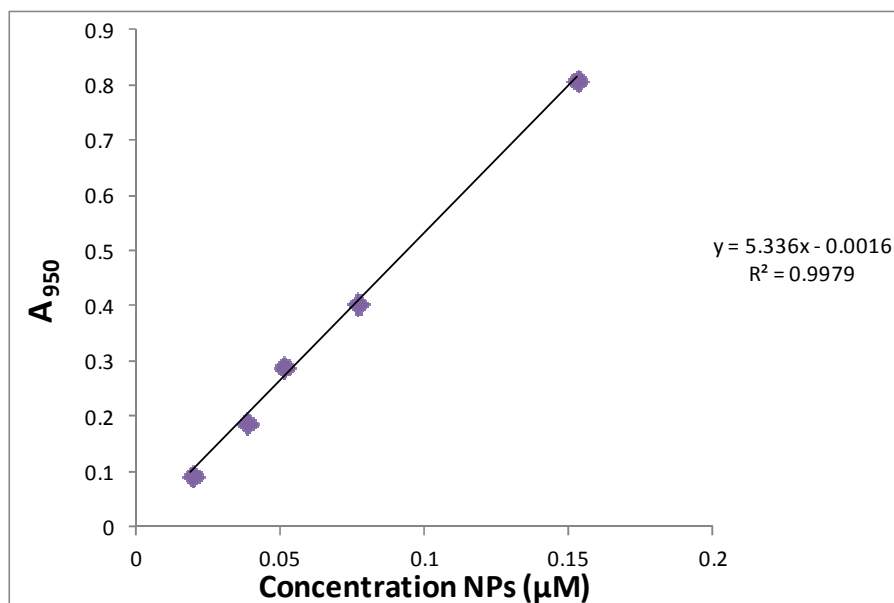


Figure S17. Standard curve for the absorbance at 950 nm of different NPs concentrations in chloroform.

5. Cell culture and laser irradiation

3T3 embryonic fibroblasts were incubated over night at 37 °C, 5 % CO_2 in growth medium (DMEM-F12 basal medium supplemented with 10 % FBS, 1 % L-glutamine, 1 % penicillin/streptomycin). The next day the cells were incubated with water soluble CuTe nanocubes at a final concentration of 75 nM for 3h. Afterwards, the medium was washed away to remove free nanoparticles and the cells were placed in a solution of 100 μM DAPI (4',6-diamidino-2-phenylindole) in PBS. DAPI is an impermeant dye commonly used to stain the nucleus. DAPI enters the cell faster when the cellular and nuclear membrane are damaged than when the cells are viable. We took advantage of this and incubated the cells in a solution of DAPI. Immediately after addition and within 10 min the images before and after NIR laser irradiation were taken.

The microscopic set up consisted of a wide-field fluorescence microscope coupled to a continuous diode laser emitting at 830 nm. The maximum output of the laser is 130 mW. However the maximum light power reaching the sample using a 100x/1.3 oil immersion objective was measured to be around 19 mW. The area of the spot was 38 μm^2 . With a tunable power supply the output power of the laser can be varied smoothly from 0 to 19 mW effective light power on the sample plane.

Cells containing the CuTe nanocubes were irradiated with 90 % maximum intensity during 1-2 s with the laser. The final intensity of the laser was 0.5 $\text{mW}/\mu\text{m}^2$. As a control for laser illumination, cells free of nanoparticles were treated as described before.

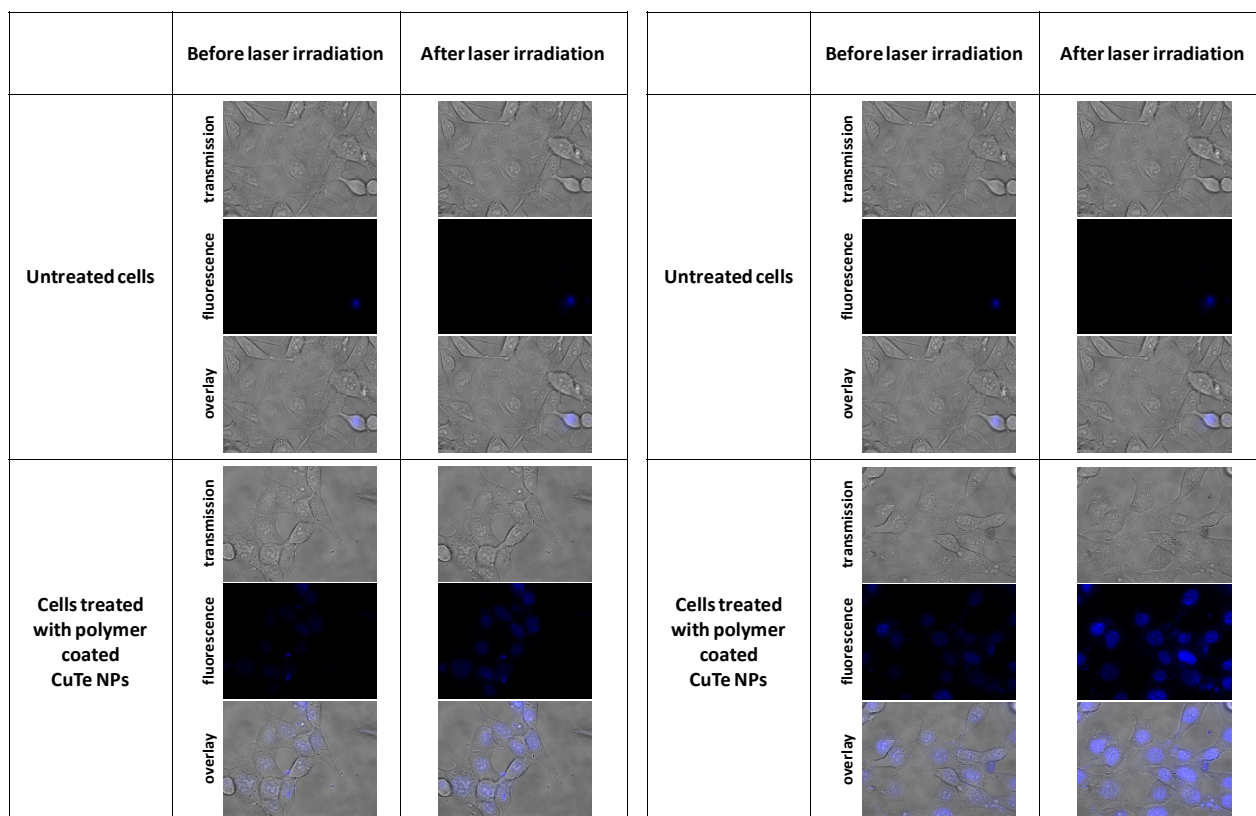


Figure S18. CuTe nanocubes-induced disruption of cell viability in two different regions.

References

- (1) Carmalt, C. J.; Compton, N. A.; Errington, R. J.; Fisher, G. A.; Moenandar, I.; Norman, N.C.; Whitmire, K. H. *In Inorganic syntheses*; Alan, H. C., Ed. **1997**, 98
- (2) Álvarez-Puebla, R. A. *J. Phys. Chem. Lett.* **2012**, *3*, 857.
- (3) Pellegrino, T.; Manna, L.; Kudera, S.; Liedl, T.; Koktysh, D.; Rogach, A. L.; Keller, S.; Radler, J.; Natile, G.; Parak, W. J. *Nano Letters* **2004**, *4*, 703.
- (4) Lin, C.-A. J.; Sperling, R. A.; Li, J. K.; Yang, T.-Y.; Li, P.-Y.; Zanella, M.; Chang, W. H.; Parak, W. J. *Small* **2008**, *4*, 334.
- (5) Guardia, P.; Di Corato, R.; Lartigue, L.; Wilhelm, C.; Espinosa, A.; Garcia-Hernandez, M.; Gazeau, F.; Manna, L.; Pellegrino, T. *ACS Nano* **2012**, *6*, 3080.
- (6) Rivera_Gil, P.; Jimenez De Aberasturi, D.; Wulf, V.; Pelaz, B.; Del Pino, P.; Zhao, Y.; De La Fuente, J. M.; Ruiz De Larramendi, I.; Rojo, T.; Liang, X.-J.; Parak, W. J. *Accounts of Chemical Research* **2012**.